

# Transient intermediate in the formation of an amorphous metal–organic framework

## SUPPLEMENTARY INFORMATION

Adam F. Sapnik,<sup>1</sup> Michael F. Thorne,<sup>1</sup> Celia Castillo-Blas,<sup>1</sup> Luke Keenan,<sup>2</sup> Timothy Johnson<sup>3</sup> and  
Thomas D. Bennett.<sup>1\*</sup>

<sup>1</sup> Department of Materials Science and Metallurgy, University of Cambridge, Cambridge, CB3 0FS, UK.

<sup>2</sup> Diamond Light Source Ltd, Diamond House, Harwell Campus, Didcot, Oxfordshire, OX11 0DE, UK.

<sup>3</sup> Johnson Matthey Technology Centre, Blount's Court, Sonning Common, RG4 9NH, UK.

\* To whom correspondence should be addressed; E-mail: [tdb35@cam.ac.uk](mailto:tdb35@cam.ac.uk)

## Methods and Materials

### Chemicals

All chemicals were obtained from commercial suppliers and used as received. Iron (III) nitrate nonahydrate (99.95%), 1,3,5-benzenetricarboxylic acid (95%), methanol (99.8%), ethanol (99.8%), ammonium fluoride (99.99%) and Fe standards were all purchased from Sigma Aldrich.

### Fe-BTC powder synthesis

Powdered samples of Fe-BTC were synthesised following the method reported in Ref. 1. Iron (III) nitrate nonahydrate (2.5988 g, 6.43 mmol) and 1,3,5-benzenecarboxylic acid (1.1770 g, 5.60 mmol) were each dissolved in 20 mL of methanol. The two solutions were combined at room temperature and left to stir overnight. The powder was then washed, purified and dried. Pellets of Fe-BTC were formed by first grinding Fe-BTC powder with cellulose (20  $\mu\text{m}$ ) in an agate pestle and mortar for 15 min. The intimately ground mixture was then transferred to a circular pellet die (13 mm diameter) and compounded under 10 tonnes of pressure for 5 minutes. The mass of the samples was calculated in the XAFS<sub>mass</sub> software to optimise for an edge step of 0.9 to 1.1.<sup>2</sup>

### Fe standards

Fe standards of various oxidation states and ligand environments were made into methanolic solutions or pellets (following the method described above), depending on the solubility of the standard. In total, ten pellets and two solutions were used alongside Fe foil.

### *In-Situ* Fe-BTC gel synthesis

Fe-BTC gel was synthesised following a method adapted from Ref. 1. Specifically, methanolic stock solutions of iron (III) nitrate (37.5 mmol L<sup>-1</sup>) and 1,3,5-benzenetricarboxylic acid (150 mmol L<sup>-1</sup>) were produced and then chilled to *ca.* 5°C in an acetone–ice bath for 1 hour. The reduced concentrations were employed to achieve an edge step close to unity. The reaction vessel was placed in an acetone–ice bath and 80 mL of the metal solution was placed into the vessel and circulated through a Kapton capillary in the path of the beam *via* tubing connected to a peristaltic pump. Next, 20 mL of the organic linker solution was loaded into two syringes connected to a pump (*i.e.*, 10 mL in each) and injected into the metal solution to initiate the reaction.

### X-ray absorption spectroscopy

X-ray absorption spectroscopy (XAS) was performed at the Fe K-edge (7112 eV) using the I20-EDE beamline at Diamond Light Source (UK) (experiment number SP28536-1).<sup>3,4</sup> I20-EDE is an energy-dispersive EXAFS beamline that was optically optimised at the Fe absorption edge (7112 eV), in transmission mode and is optimised for rapid data collection at the sacrifice of energy resolution and *k*-range. The storage ring energy was 3 GeV and was operated at 300 mA in top-up mode (with an injection period of 20 seconds every 10 mins). The synchrotron radiation from an 8-pole wiggler insertion device (18.5 mm gap between 1.2 T magnets) is conditioned with an initial aperture of size 0.77 mm x 0.84 mm (h x v) and beam-defining primary slits of 1.5 mrad horizontally and 0.1 mrad vertically. In horizontal the beam is focused using a curved Si(111) polychromator (radius of curvature = 12.0 m) in Bragg geometry.<sup>5</sup> This curvature leads to a polychromatic beam with the energy range at the sample measured was 7040 to 7640 eV. The beam is vertically focused by a curved mirror ME1 at 36 m from the beam source (radius of curvature = 8.6 km) with a Rh coating and 3.1 mrad pitch angle. The unwanted low energies were filtered out using two Be windows of 300  $\mu\text{m}$  thickness along the

beamline and the high energies were removed by harmonic rejection mirrors with a silicon coating at 3.0 mrad pitch angle. This gave a beam size of 40 x 200  $\mu\text{m}$  (FWHM h x v) at the focal spot on the sample position. To remove the background a reference sample of methanol without Fe was measured before each XAS measurement. The detector used was the FReLoN CCD (14  $\mu\text{m}$  per pixel),<sup>6</sup> with a typical measurement of 0.5 s per spectrum. The detector's pixel-to-energy calibration was calculated by measuring a 5  $\mu\text{m}$  thick Fe foil and comparing to the same foil measured on the monochromatic XAS beamline, I20-SCANNING, at Diamond Light Source. and rechecked daily during the experiment. The overall result is that the whole X-ray absorption spectrum to be collected simultaneously. Additionally, the size of the focussed beam at the sample position is very stable (+/-1  $\mu\text{m}$  horizontal and +/-10  $\mu\text{m}$  vertical beam position) as there is no requirement for the optical elements to be moved during the data collection.

*In-situ* measurements were collected with a time resolution of 0.5 s per spectra for 5 min, resulting in a total of 600 spectra. Injection of the linker solution to the metal solution took 3 s and was initiated after 20 s (40<sup>th</sup> spectra). Static measurements of the pelleted samples were collected using an acquisition time of approximately 2.5 ms in a similar manner to the *in-situ* data.

Data were processed in DAWN,<sup>7</sup> where a flat background from the pre-edge slope and a fitted low-order Chebyshev polynomial to the post-edge region were both subtracted. The Fourier transform and phase correction of the normalised data were performed in Athena.<sup>8</sup> The XANES spectrum of Fe(II)-BTC was calculated from the reported structure using the DFT FDMNES software on the Diamond Light Source cluster computer.<sup>9</sup>

#### Avrami-Erofeev model

$\alpha$  is the reaction coordinate,  $k$  is the rate constant of formation,  $t$  is time and  $n$  is the Avrami constant.

$$\alpha = 1 - \exp[-(kt)^n]$$

#### Gualtieri model

$\alpha$  is the reaction coordinate,  $k_G$  is the rate of crystal growth,  $n_G$  is the dimensionality constant,  $a_N$  is the reciprocal of the nucleation rate  $k_N$ ,  $P_N$  describes the nucleation probability distribution and is derived as follows  $P_N = \exp[-(t - a)^2/2b^2]$ .

$$\alpha = \frac{1 - \exp[-(k_G t)^{n_G}]}{1 + \exp\left[-\left(\frac{t - a_N}{b_N}\right)^2\right]}$$

#### Sharp-Hancock model

$\alpha$  is the reaction coordinate,  $k$  is the rate constant of formation,  $t$  is time and  $n$  is the Avrami constant.

$$-\ln \ln(1 - \alpha) = n \ln k + n \ln t$$

## UV-vis spectroscopy

*In-situ* UV-Vis measurements were performed using an Agilent Cary 60 UV-Vis spectrophotometer in the range 300–800 nm. Samples were measured in rectangular polystyrene cuvettes with a path length of 1 cm and a total volume of 3.5 mL. The reaction concentration described for Fe-BTC powder synthesis was reduced by a factor of 80 to reduce absorbance to measurable values (iron (III) nitrate at 4.02 mmol L<sup>-1</sup> and trimesic acid at 3.5 mmol L<sup>-1</sup>). 1.75 mL of each stock solution was combined in the cuvette. Spectra were acquired using an averaging time of 0.0125 s, an integration of 5 nm and a scan rate of 24,000 nm min<sup>-1</sup>. Each spectrum took 6 s to collect, and spectra were acquired for 45 min resulting in a total of 450 spectra.

## Powder X-ray diffraction

Data were collected at room temperature using a Bruker D8 diffractometer using Cu K $\alpha_1$  ( $\lambda = 1.5406 \text{ \AA}$ ) radiation and a LynxEye position-sensitive detector with Bragg-Brentano parafocusing geometry. Samples of finely ground powder were dispersed onto a low background silicon substrate and loaded onto the rotating stage of the diffractometer. Data were collected over the angular range  $5^\circ < 2\theta < 50^\circ$ .

## Supplementary Figures

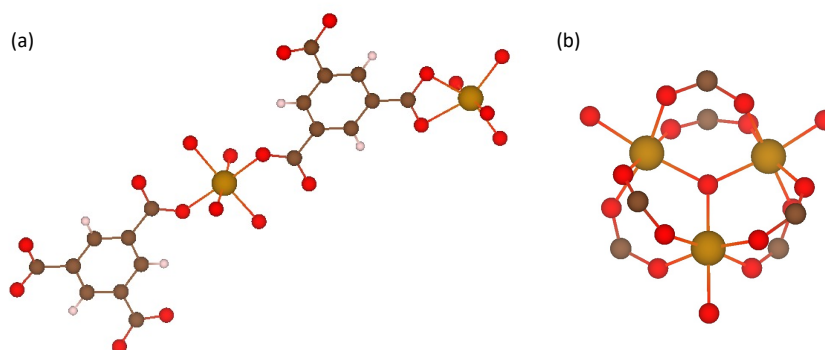


**Figure S1** Local structure of (a) Fe(II)-BTC and (b) Fe-BTC. In (a) the carboxylate anions bind in either a bridging ( $\mu^1$ ) or chelate ( $\mu^2$ ) mode. Fe (orange), O (red), C (brown) and H (white).

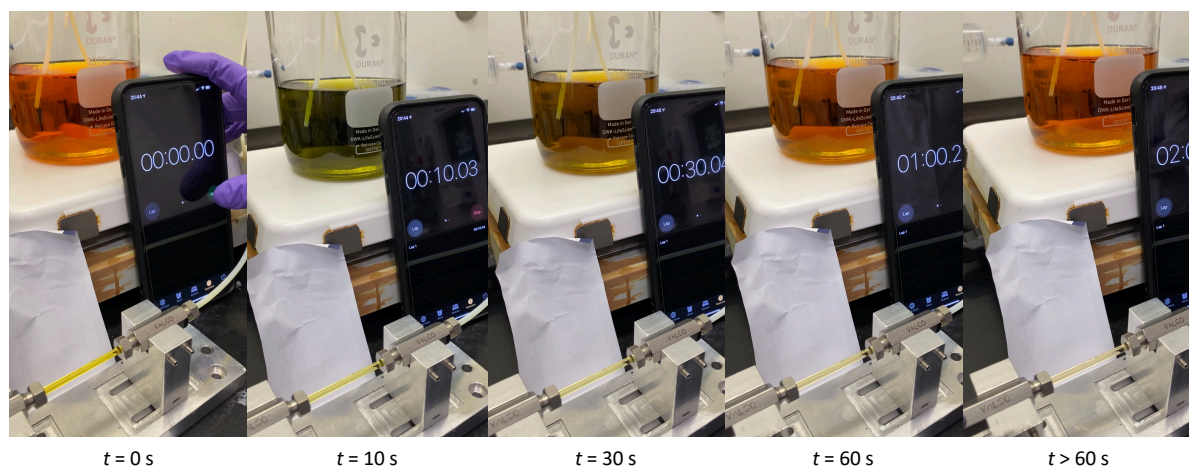


**Figure S2** Time-resolved photoset of the Fe-BTC reaction at room temperature. In the background the reaction vessel can be seen, this solution is pumped *via* a peristaltic pump (not pictured) through the quartz capillary in the foreground. The timer was started upon addition of the linker solution to the metal solution. After 10 seconds the solution was green, yellow after 30 seconds and returned back to orange after 60 seconds. No further colour changes were observed after 60 seconds.

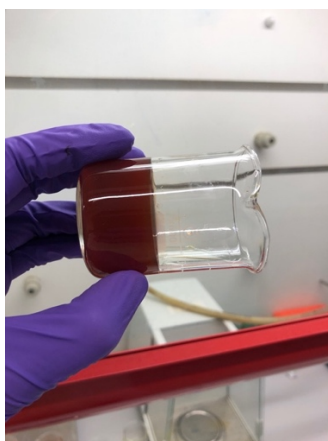


**Figure S3** Image of the Fe-BTC reactant mixture at the 'Fe-BTC powder synthesis' concentration, as reported in Ref. 1.

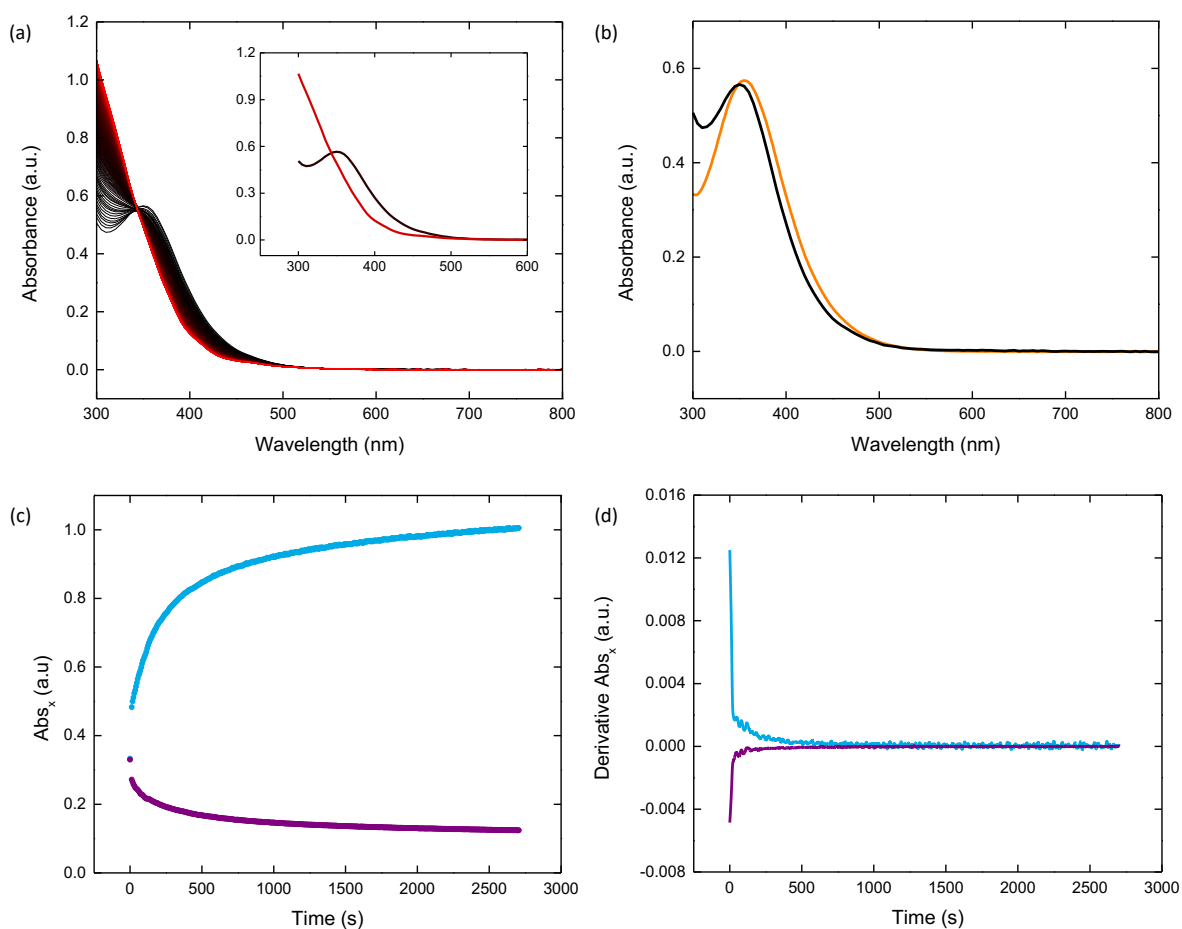


**Figure S4** (a) *In-situ* UV-vis absorption spectra for the formation of Fe-BTC over 45 minutes (black to red). Inset shows the spectra for  $t = 12$  s (black) and  $t = 2700$  s (red) after mixing (b) Comparison between the first spectrum obtained from the *in-situ* measurement at  $t = 12$  s after mixing (black) and an iron (III) nitrate standard solution (orange). (c) Absorbance as a function of time for  $\lambda = 300$  nm (blue) and  $\lambda = 400$  nm (purple). (d) Derivative of the absorbance as a function of time for  $\lambda = 300$  nm (blue) and  $\lambda = 400$  nm (purple).

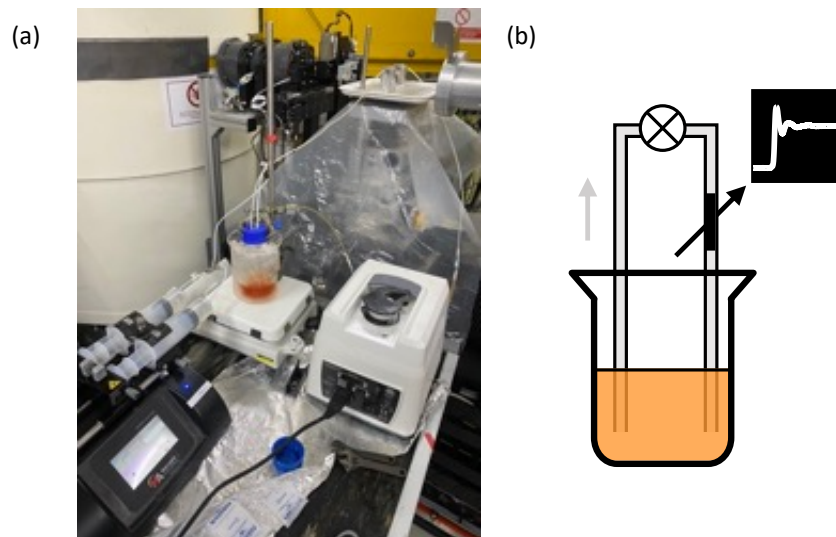


**Figure S5** Experimental setup used for the *in-situ* measurements. **(a)** The syringe pump injects the linker solution into the reaction vessel which contains the metal solution and is submerged within an acetone–ice bath. The reaction solution is circulated through a quartz capillary in the path of the beam by the peristaltic pump. **(b)** Schematic of the experimental set-up. The peristaltic pump (circular icon) pumps the reaction solution in the direction of the grey arrow. As the solution passes through the Kaptan capillary (black region), synchrotron X-rays (black arrow) are passed through the sample and absorption spectra are collected.

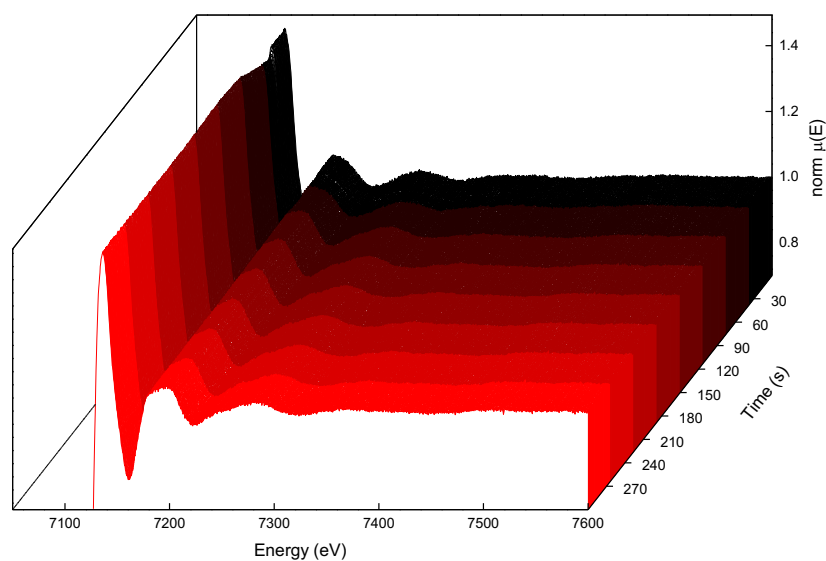


**Figure S6** The complete *in-situ* dataset collected for the formation of Fe-BTC over five minutes. The linker solution was added at  $t = 20$  s.

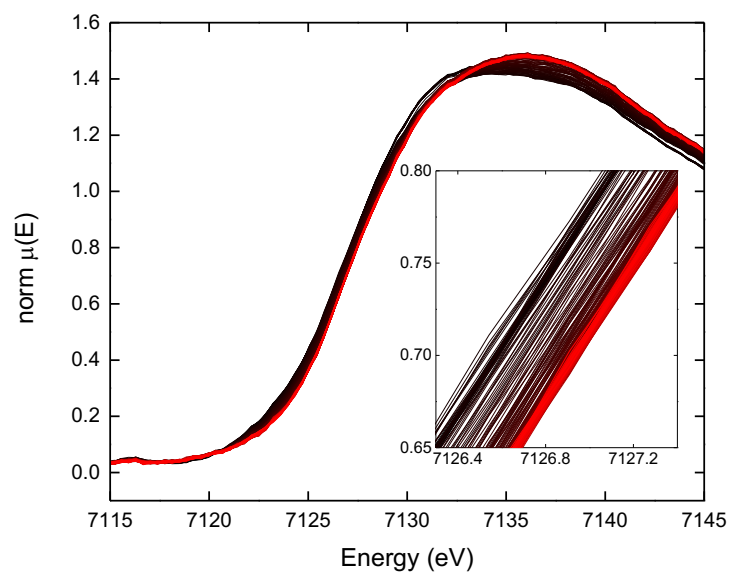


**Figure S7** Rising edge of the *in-situ* XANES data (black to red) collected over five minutes. Inset shows the shift in position at the half-maximum of the white line. There is an initial shift towards lower energy followed by a shift towards higher energy.

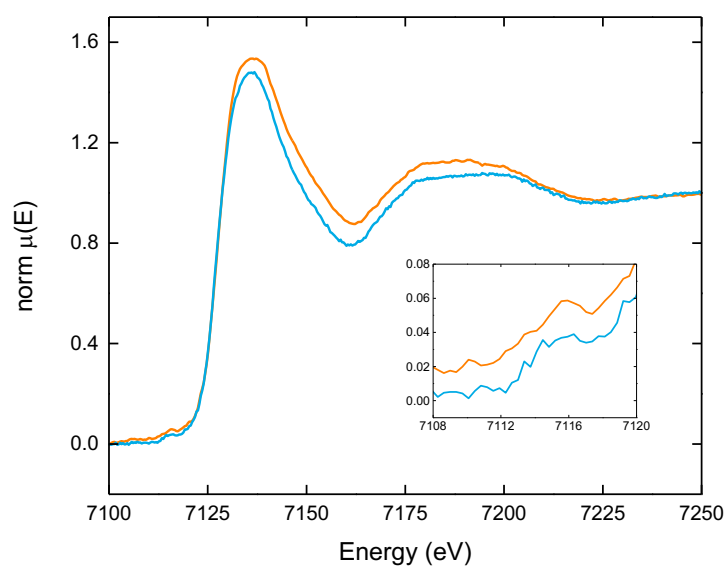


**Figure S8** Comparison between the XANES and pre-edge (inset) regions of the spectra for Fe-BTC in pellet (orange) and solution (blue) form.

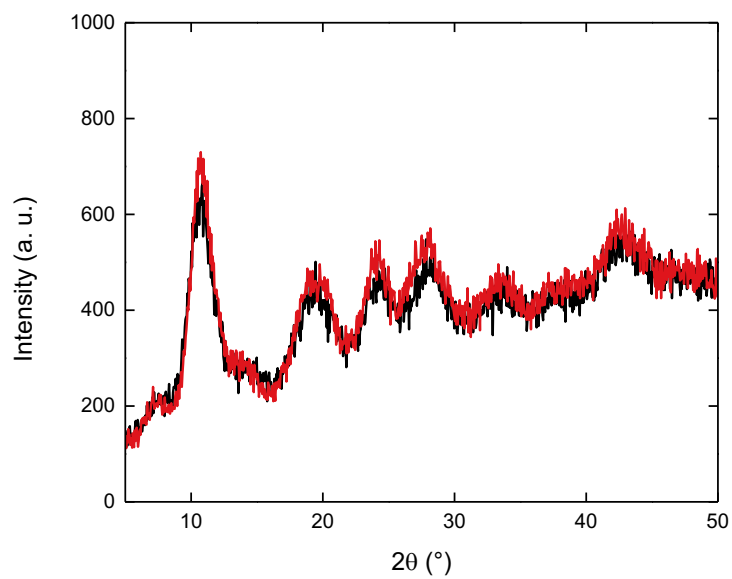


**Figure S9** Powder X-ray diffraction data for Fe-BTC synthesised from the *in-situ* experiment (black), compared to Fe-BTC as reproduced from Ref. 1 (red).

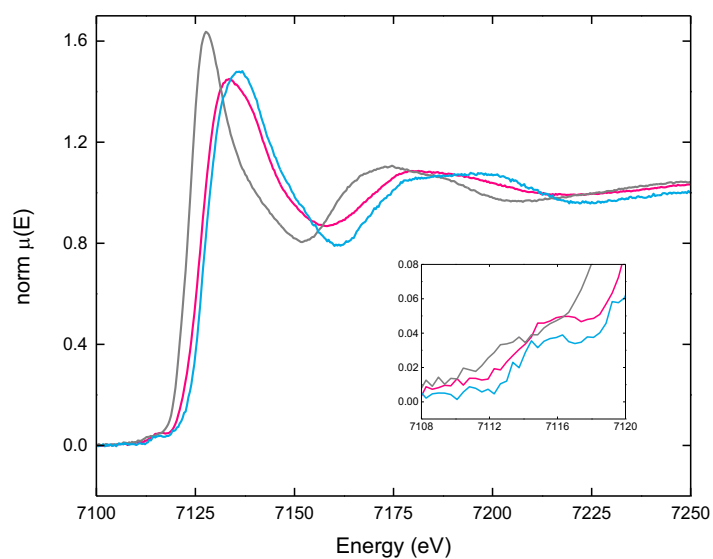


**Figure S10** Comparison between the XANES and pre-edge (inset) regions of the spectra for Fe-BTC solution (blue),  $\text{Fe}(\text{NO}_3)_3$  solution (pink), and  $\text{FeCl}_2$  solution (grey).

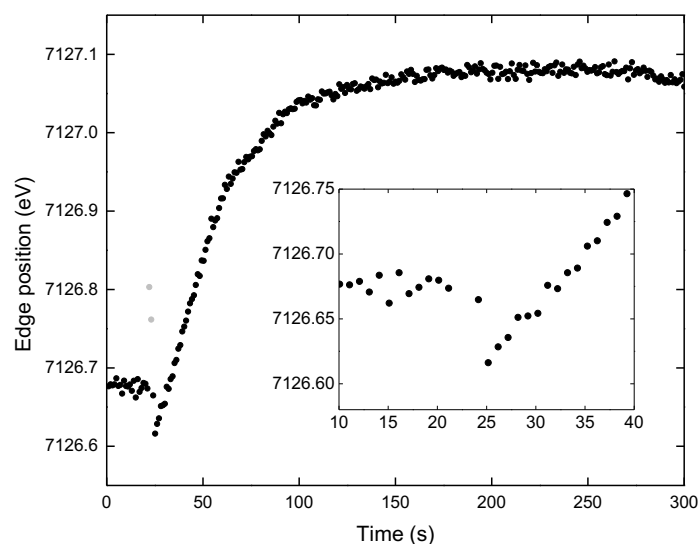


**Figure S11** Evolution of the rising edge position during the formation of Fe-BTC over the course of five minutes. Inset shows the variation upon mixing, which occurs at  $t = 20$  s. The delay between  $t = 20$  s and  $t = 25$  s can be attributed to the mixing of the reagents and subsequent travel from the reaction vessel to the quartz capillary in the path of the beam.

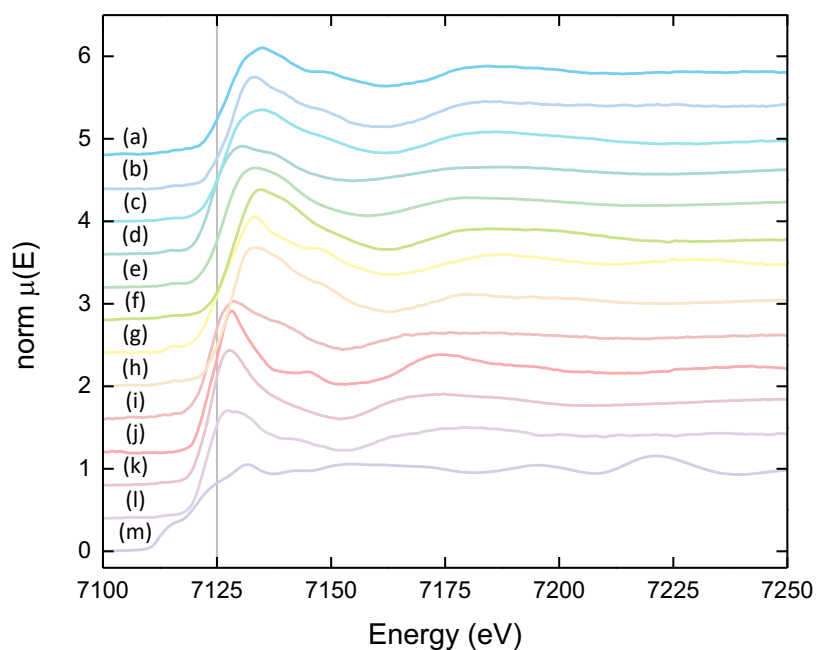


**Figure S12** Normalised spectra for (a)  $\text{Fe}_2\text{O}_3$  pellet, (b)  $\text{FeO}(\text{OH})$  pellet, (c)  $\text{Fe}(\text{ox})_3$  pellet, (d)  $\text{FeCl}_3$  pellet, (e)  $\text{Fe}(\text{NO}_3)_3$  solution, (f)  $\text{Fe}(\text{NO}_3)_3$  pellet, (g)  $\text{Fe}_3\text{O}_4$  pellet, (h)  $\text{FeCO}_3$  pellet, (i)  $\text{Fe}(\text{ac})_2$  pellet, (j)  $\text{Fe}(\text{ox})_2$  pellet, (k)  $\text{FeCl}_2$  solution, (l)  $\text{FeCl}_2$  pellet and (m) Fe foil. Pellets were made with cellulose and solutions with methanol. (ox) = oxalate and (ac) = acetate. All data offset for clarity and vertical line at  $E = 7125$  eV is a visual guide.

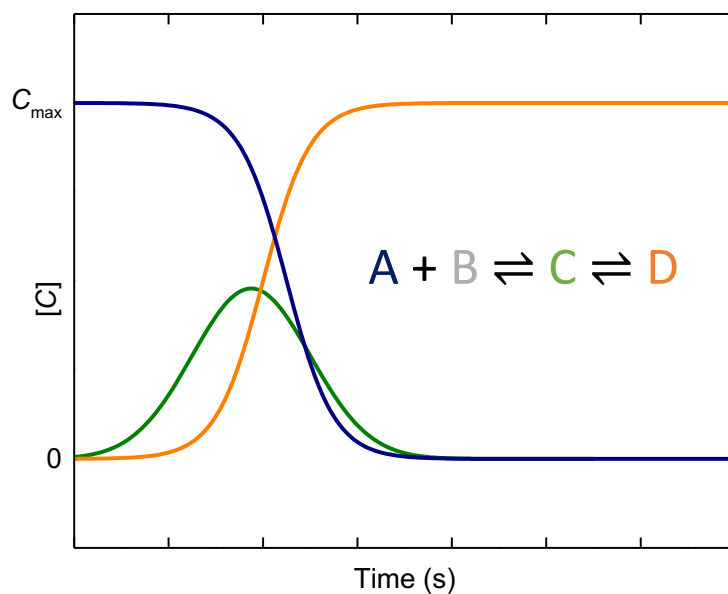


**Figure S13** Proposed reaction scheme for the formation of Fe-BTC. Anticipated variation in concentration for the reagent (blue), an intermediate (green) and the product (orange) as a function of time. A and B represent methanolic solutions of  $\text{Fe}(\text{NO}_3)_3$  and 1,3,5-benznetricarboxylic acid, respectively. C represents the equilibria associated with the intermediate and D is the final product, Fe-BTC.

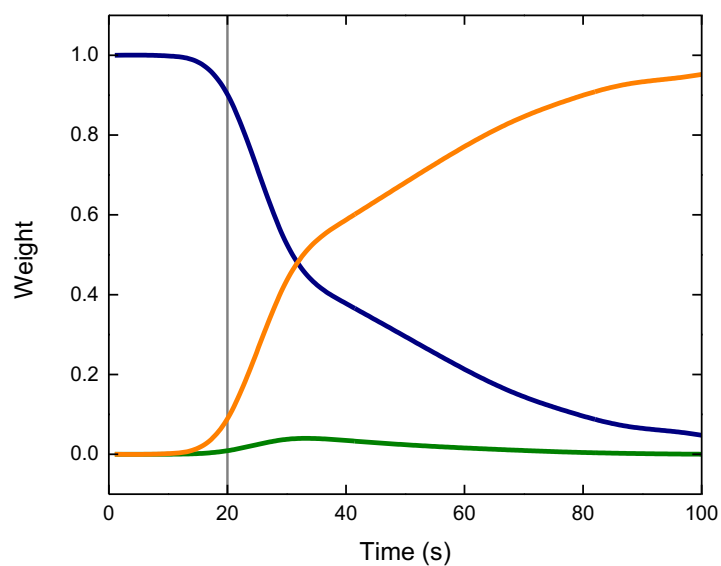


**Figure S14** Weightings obtained through LCA in the XANES region using  $\text{Fe}(\text{NO}_3)_3$  (navy), Fe-BTC (orange) and the Fe(II)-BTC (green) spectrum calculated using DFT. The vertical line marks when the reagents were combined at  $t = 20$  s.

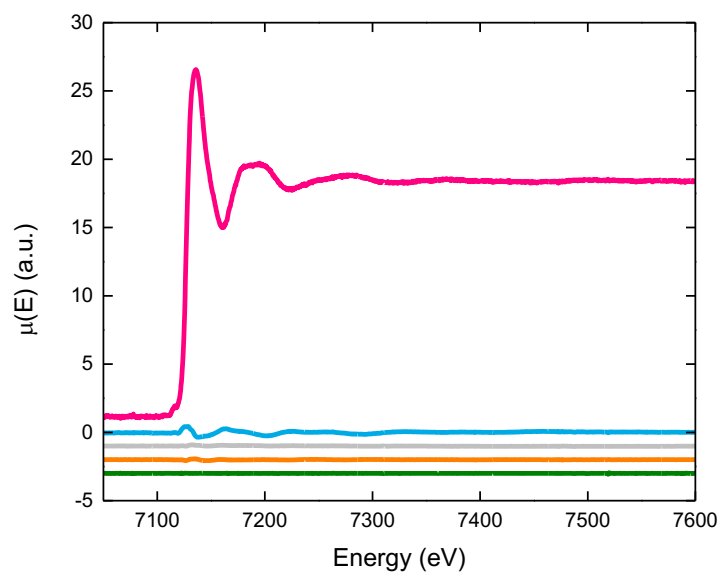


**Figure S15** Principal components obtained from the *in-situ* measurements. First (pink), second (blue), third (grey), fourth (orange) and fifth (green) components; each component offset for clarity.

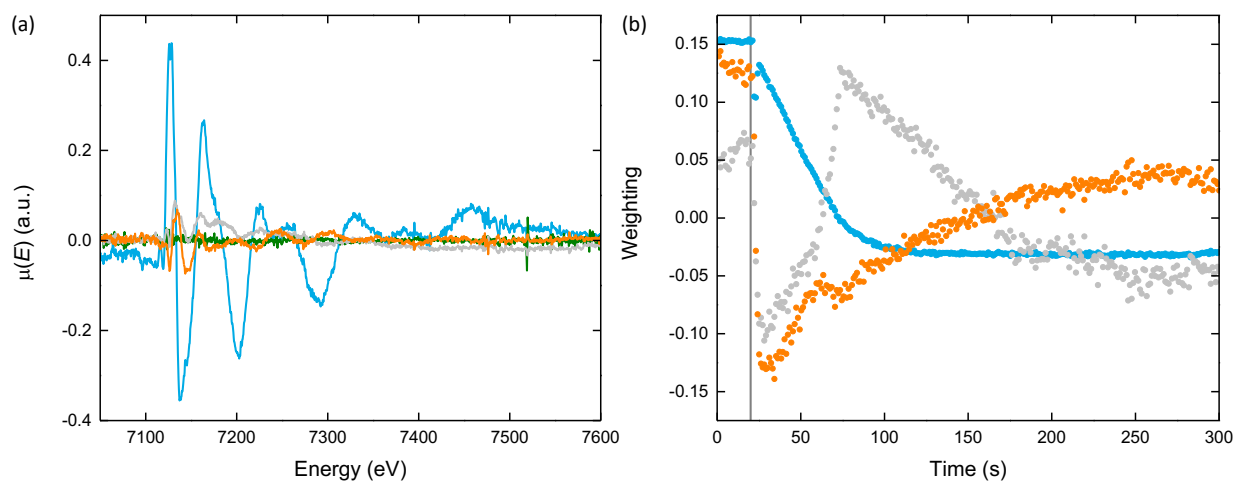


**Figure S16 (a)** The second (blue), third (grey), fourth (orange) and fifth (green) principal components determined via principal component analysis. **(b)** The corresponding weightings of the second, third and fourth principal components. The vertical line marks when the reagents were combined at  $t = 20$  s.

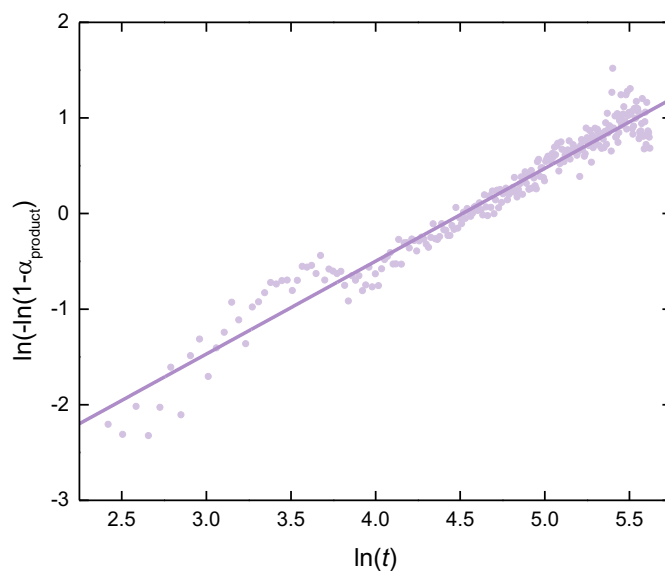


**Figure S17** Global linear Sharp-Hancock fit to  $\alpha_{\text{product}}$  – a clear change in gradient can be observed suggesting a change in mechanism occurs.

**Table S1** Summary of the kinetic parameters derived from  $\alpha_{\text{product}}$ 

Avrami analysis of $\alpha_{\text{product}}$	
$k$	$0.010 \text{ s}^{-1}$
$n$	1.00
$R$	0.97577
Gualtieri analysis of $\alpha_{\text{product}}$	
$k_N$	$0.016 \text{ s}^{-1}$
$k_G$	$0.055 \text{ s}^{-1}$
$n_G$	2.3
$R$	0.97897
Sharp-Hancock analysis of $\alpha_{\text{product}}$ (global)	
$k$	$0.011 \text{ s}^{-1}$
$n$	0.97
$R$	0.94558
Sharp-Hancock analysis of $\alpha_{\text{product}}$ ( $t < 63 \text{ s}$ )	
$k$	$0.020 \text{ s}^{-1}$
$n$	1.6
$R$	0.91189
Sharp-Hancock analysis of $\alpha_{\text{product}}$ ( $t > 73 \text{ s}$ )	
$k$	$0.010 \text{ s}^{-1}$
$n$	1.03
$R$	0.92266

## References

- (1) A. F. Sapnik, I. Bechis, S. M. Collins, D. N. Johnstone, G. Divitini, A. J. Smith, P. A. Chater, M. A. Addicoat, T. Johnson, D. A. Keen, K. E. Jelfs and T. D. Bennett, *Nat. Commun.*, 2021, **12**, 2062.
- (2) K. Klementiev and R. Chernikov, *J. Phys. Conf. Ser.*, 2016, **712**, 012008.
- (3) S. Diaz-Moreno, S. Hayama, M. Amboage, A. Freeman, J. Sutter and G. Duller, *J. Phys. Conf. Ser.*, 2009, **190**, 012038.
- (4) S. Diaz-Moreno, M. Amboage, M. Basham, R. Boada, N. E. Bricknell, G. Cibir, T. M. Cobb, J. Filik, A. Freeman, K. Geraki, D. Gianolio, S. Hayama, K. Ignatyev, L. Keenan, I. Mikulska, J. F. W. Mosselmans, J. J. Mudd and S. A. Parry, *J. Synchrotron Radiat.*, 2018, **25**, 998–1009.
- (5) H. Tolentino, E. Dartyge, A. Fontaine and G. Tourillon, *J. Appl. Cryst.*, 1988, **21**, 15–22.
- (6) J.-C. Labiche, O. Mathon, S. Pascarelli, M. A. Newton, G. G. Ferre, C. Curfs, G. Vaughan, A. Homs and D. F. Carreiras, *Rev. Sci. Instrum.*, 2007, **78**, 091301.
- (7) M. Basham, J. Filik, M. T. Wharmby, P. C. Y. Chang, B. El Kassaby, M. Gerring, J. Aishima, K. Levik, B. C. A. Pulford, I. Sikharulidze, D. Sneddon, M. Webber, S. S. Dhesi, F. Maccherozzi, O. Svensson, S. Brockhauser, G. Náray and A. W. Ashton, *J. Synchrotron Radiat.*, 2015, **22**, 853–858.
- (8) B. Ravel and M. Newville, *J. Synchrotron Radiat.*, 2005, **12**, 537–541.
- (9) O. Bunău and Y. Joly, *J. Phys. Condens. Matter*, 2009, **21**, 345501.